FEM modeling of magnetostrictive thin layers combining magnetoelastic simplified Model and shell element: application to magnetoelectric composites

Tiawen HUANG, Hakeim TALLEB, Aurélie GENSBITTEL, Zhuoxiang REN
Sorbonne Université, CNRS, Laboratoire de Génie Electrique et Electronique de Paris, 75252, Paris, France
Université Paris-Saclay, CentraleSupélec, CNRS, Laboratoire de Génie Electrique et Electronique de Paris, 91192, Gif-sur-Yvette, France.
E-mail : tianwen.huang@sorbonne-universite.fr

ABSTRACT - This paper proposes to use the nodal shell element in a FEM multiphysics formulation to simulate magnetoelectric laminate composites constituted of thin magnetostrictive layers. This study provides the basis to study the ME devices composed of laminated thin layers.

Keywords - Self-biased magnetoelectric, FEM, Shell element, magnetoelastic simplified model.

1. INTRODUCTION

Magnetoelectric (ME) materials are heterostructures that couple magnetostrictive and piezoelectric materials through elastic strain. They have the particularities to induce an electric polarization by a magnetic field or vice versa, making them suitable for engineering applications such as sensors or actuators [1], [2]. Among the promising applications, we can cite particularly the use as energy transducers for supplying power to implanted electronic devices in the biomedical domain through magnetic wireless powering [3], [4]. In most cases, the magnetic excitation is composed of a small dynamic magnetic signal H_{ac} around a fixed static bias magnetic field H_{DC} where the ME response is maximal. Nevertheless, the use of H_{DC} requires permanent magnets, which poses a significant inconveniency for developing implanted electronic devices. In this context, the self-biased ME (SME) composites based on magnetostrictive film materials such as Nickel (Ni) are attractive since they are compact while presenting a remarkable remanent ME response without a static bias magnetic field [5].

This paper proposes an investigation into two different combinations of laminate magnetoelectric composites (MECs): SME Ni/(YXl)163° $LiNbO_3$ (10×5×0.1 mm^3)/Ni composite and non SME Ni/PZT-5H (11×5×0.22 mm^3)/Ni composite. The nickel (Ni) films with a thickness of approximately 10 µm, were deposited using RF sputtering. The primary focus of this study is on the ME L-T working mode as depicted in Fig. 1, where magnetic excitation is applied longitudinally and electric voltage *V* is induced transversally, the efficiency of the MECs is commonly measured using the magnetoelectric coefficient ($\alpha_E = \delta V/(\delta H_{ac} \cdot t_p)$), where t_p is the thickness of the piezoelectric layer. The investigation utilizes a numerical code based on the Finite Element Method (FEM) as multiphysics tool for analysis. We employ the nodal shell element principle to effectively consider the magnetoelastic coupling of the thin magnetostrictive Ni material, capturing the dominant in-plane behavior while neglecting the out-of-plane effects. Furthermore, a simplified magnetoelastic anhysteretic model is incorporated into the FEM formulation to account for the non-linear behavior of the Ni material. To ensure the accuracy of the multiphysics tool, simulation results under both static and dynamic regimes are compared against experimental findings for validation purposes.

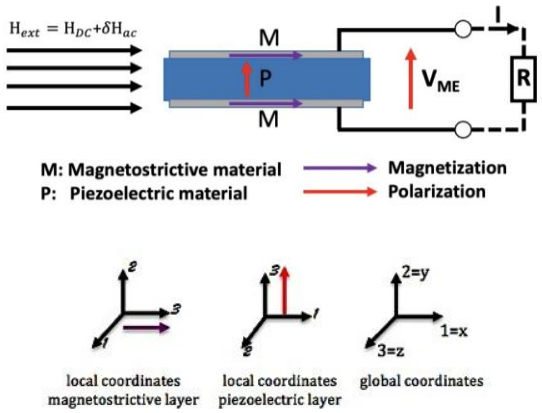

Fig. 1. The studied ME composite exicited in L-T mode.

2. FEM MODELING USING SHELL ELEMNT

2.1. Governing equations

The equilibrium and the compatibility equations for a magnetoelectric problem are respectively given by (1) and (2):

$$\begin{aligned} div\boldsymbol{T} + \boldsymbol{f} &= \rho_v \partial_t^2 \boldsymbol{u} \\ \text{div}\boldsymbol{D} &= \rho \\ \text{curl}\ \boldsymbol{H} &= \boldsymbol{J} \end{aligned} \tag{1}$$

where $\boldsymbol{f}$ is the body force, ρ is the electrical charge and $\boldsymbol{J}$ is the free current density. $\boldsymbol{T}$, $\boldsymbol{D}$ and $\boldsymbol{H}$ represent respectively the mechanical stress tensor, electric displacement field and magnetic field. Finally, $\boldsymbol{u}$, $\boldsymbol{f}$ and ρ_v are respectively the mechanical displacement, the externally applied volume force and the mass density of the medium. In this study, we consider $\rho = 0$ and $\boldsymbol{J} = 0$.

$$\begin{aligned} \boldsymbol{S} &= \frac{1}{2}(grad(\boldsymbol{u}) + grad^T(\boldsymbol{u})) \\ \text{curl}\ \boldsymbol{E} &= 0 \\ \text{div}\boldsymbol{B} &= 0 \end{aligned} \tag{2}$$

where $\boldsymbol{S}$, $\boldsymbol{E}$ and $\boldsymbol{B}$ are respectively the mechanical strain, the electric field and the magnetic induction.

The coupled constitutive equations for a MEC can be written as follows:

$$\begin{bmatrix} \boldsymbol{T} \\ \boldsymbol{D} \\ \boldsymbol{H} \end{bmatrix} = \begin{bmatrix} (\mathbb{c}^{\boldsymbol{E}} + \mathbb{c}^{\boldsymbol{B}}) & -\mathbb{e}^{\mathrm{T}} & -\mathbb{h}^{\mathrm{T}} \\ -\mathbb{e} & \mathbb{p}^{S} & 0 \\ -\mathbb{h} & 0 & \mathbb{v}^{S} \end{bmatrix} \begin{bmatrix} \boldsymbol{S} \\ \boldsymbol{E} \\ \boldsymbol{B} \end{bmatrix} \tag{3}$$

Here, the symmetric tensors $\mathbb{e}$ and $\mathbb{h}$ contain the piezoelectric and piezomagnetic material coefficients, respectively. The diagonal elements $\mathbb{c}^{\boldsymbol{E}}$ and $\mathbb{c}^{\boldsymbol{B}}$ represent the stiffness tensors of piezoelectric and magnetostrictive elements under constant electric field and constant magnetic induction, respectively. The $\mathbb{p}^{S}$ and $\mathbb{v}^{S}$ are the permittivity under constant strain and the reluctivity under constant strain, respectively.

Once the coupled magnetoelectric problem with a 2D assumption [6]–[8] has been discretized into finite elements, the unknown variables of the problem consist of the mechanical displacement $\boldsymbol{u} = \{u_x, u_y\}$, the electric potential V, and the z-component of the magnetic potential a_z at the mesh nodes. The fields $\boldsymbol{S}$, $\boldsymbol{E}$ and $\boldsymbol{B}$ are then expressed in matrix form using the derivatives of the nodal shape functions $N_{u,v,a}$.

$$\begin{bmatrix} \boldsymbol{S} \\ \boldsymbol{E} \\ \boldsymbol{B} \end{bmatrix} = \begin{bmatrix} \mathrm{G_u} & 0 & 0 \\ 0 & \mathrm{G_v} & 0 \\ 0 & 0 & \mathrm{G_a} \end{bmatrix} \begin{bmatrix} \boldsymbol{u} \\ V \\ a_z \end{bmatrix} \tag{4}$$

where $\mathrm{G_u} = \frac{1}{2}\left(grad_{\mathrm{xy}} + grad_{\mathrm{xy}}{}^{\mathrm{T}}\right)[N_u] = D[N_u]$, $\mathrm{G_V} = \mathrm{grad_{xy}}[N_v]$, $\mathrm{G_a} = \mathrm{r}^{*} grad_{\mathrm{xy}}[N_a]$ are gradient operators with $r^{*} = [0 \quad 1, -1 \quad 0]^{\mathrm{T}}$ a rotation matrix in Cartesian coordinates.

2.2. *Modeling of thin magnetostrictive layer*

When MECs are composed of thin layers and thick layers [9], the thickness of the magnetostrictive layer (δ) is typically much smaller than the dimension of the piezoelectric layer, which includes its thickness (t_p) and length (L_x) (usually δ/A <10-3, where $A = \max(\|t_p\|) \cup \|L_x\|$). Traditional finite element modeling of such structures requires an extremely fine mesh to prevent mesh distortion and maintain accuracy, which can be time-consuming, and since the magnetostrictive behavior is primarily driven by in-plane deformations, to simplify this process, an effective thin layer can be considered for the magnetostrictive layer and modeled using a line element [10]. The nodes of the line element are duplicated, as shown in Fig. 2, using the gradient approximation proposed in [11] to degenerate the 3-node linear triangular element into a 2-node line element.

$$\begin{aligned} grad_L[N\emptyset] = \frac{1}{2}\frac{\partial}{\partial x}\left(\sum_{i=1}^{2} N_i^0 \langle \emptyset_i \rangle\right)\overrightarrow{e_x} \\ + \frac{1}{\delta}\left(\sum_{i=1}^{2} N_i^0 [\emptyset_i]\right)\overrightarrow{e_y} \end{aligned} \tag{5}$$

where $\langle \emptyset_i \rangle = \emptyset_i^{+} + \emptyset_i^{-}$ and $[\emptyset_i] = \emptyset_i^{+} - \emptyset_i^{-}$ are, respectively, the weighted average and the jump of unknown variable $\emptyset_i$ along and across the thickness δ. The annotations $\emptyset_i^{+}$ and $\emptyset_i^{-}$ represent the nodal values of $\emptyset_i$ on both sides of the thin layer element and N_i^0 is the shape function for 2-node line element.

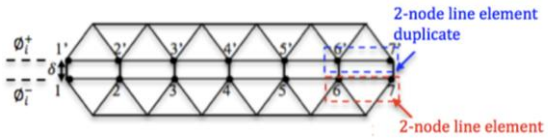

Shell nodal elements introduced in duplicate the 2-node line element

Fig. 2. Illustration of the method to consider thin layer.

As a result, we model the effective thin layer using symmetric 4-node elements (Q4 element), which approximate the unknown variables $\boldsymbol{u} = \{u_x, u_y\}$, V, and a_z using shape functions (6) and (7). These functions are obtained by degenerating the 2-node line element.

$$\{\boldsymbol{u}\} = N_{ui}^0 \boldsymbol{u_i}, \{V\} = N_i^0 V_{\boldsymbol{i}}, \{a_z\} = N_i^0 \, a_{z_{\boldsymbol{i}}}$$

with the shape functions

$$N_{ui}^0 = \begin{bmatrix} N_1{}' & 0 & N_2{}' & 0 & 0 & 0 & 0 & 0 \\ 0 & N_1{}' & 0 & N_2{}' & 0 & 0 & 0 & 0 \\ 0 & 0 & 0 & 0 & N_1{}' & 0 & N_2{}' & 0 \\ 0 & 0 & 0 & 0 & 0 & N_1{}' & 0 & N_2{}' \end{bmatrix} \tag{6}$$

$$N_i^0 = \begin{bmatrix} N_1{}' & 0 & N_2{}' & 0 \\ 0 & N_1{}' & 0 & N_2{}' \end{bmatrix} \tag{7}$$

where $N_1{}' = 1 - \frac{x}{L_e}$, $N_2{}' = \frac{x}{L_e}$ and L_e denotes the length of the 2-node line element.

The unknown variables are decomposed as

$$\begin{aligned} \boldsymbol{u_i} &= \{u_{x1}^{+} \quad u_{y1}^{+} \quad u_{x2}^{+} \quad u_{y2}^{+} \quad u_{x1}^{-} \quad u_{y1}^{-} \quad u_{x2}^{-} \quad u_{y2}^{-}\} \\ \boldsymbol{V_i} &= \{V_1^{+} \quad V_1^{-} \quad V_2^{+} \quad V_2^{-}\}^T \\ \boldsymbol{a_i} &= \{a_1^{+} \quad a_1^{-} \quad a_2^{+} \quad a_2^{-}\}^T \end{aligned} \tag{8}$$

And the degenerate gradient operators G_u^{shell}, G_V^{shell} and G_a^{shell} are given by:

$$\begin{aligned} G_u^{shell} &= D'^{[N_{ui}^0]} \\ G_V^{shell} &= G_a^{shell} = grad_L[N_i^0] \end{aligned} \tag{9}$$

with $D' = \begin{bmatrix} \frac{1}{2}\frac{\partial}{\partial x} & 0 & \frac{1}{2}\frac{\partial}{\partial x} & 0 \\ 0 & \frac{1}{\delta} & 0 & -\frac{1}{\delta} \\ \frac{1}{\delta} & \frac{1}{2}\frac{\partial}{\partial x} & -\frac{1}{\delta} & \frac{1}{2}\frac{\partial}{\partial x} \end{bmatrix}$ and $grad_L = \begin{bmatrix} \frac{1}{2}\frac{\partial}{\partial x} & \frac{1}{2}\frac{\partial}{\partial x} \\ \frac{1}{\delta} & -\frac{1}{\delta} \end{bmatrix}$

2.3. *Finite element formulation*

After the FEM discretization, the general coupling system equation is expressed as [6]–[8]:

$$[\mathcal{M}]\{\ddot{\mathcal{X}}\} + [\mathcal{C}]\{\dot{\mathcal{X}}\} + [\mathcal{K}]\{\mathcal{X}\} = [\mathcal{F}] \tag{10}$$

where $[\mathcal{K}]$ is the electro-magneto-mechanical stiffness matrix, $[\mathcal{C}]$ the mechanical damping matrix, $[\mathcal{M}]$ the mechanical mass matrix, $\{\mathcal{X}\}$ the unknown vector and $\{\mathcal{F}\}$ the excitation vector. In the case where the linear triangular elements are used, the submatrices in $[\mathcal{K}]$ can be formulated as [6], [7]:

$$\begin{bmatrix} K_{uu} \\ K_{pp} \\ K_{aa} \end{bmatrix} = \sum_e \int_{\Omega_e} \begin{bmatrix} [G_u]^t \mathbb{c} [G_u] \\ [G_p]^t \mathbb{p} [G_p] \\ [G_a]^t \mathbb{v} \, [G_a] \end{bmatrix} d\Omega \tag{11}$$

and

$$\begin{bmatrix} K_{up} \\ K_{ua} \end{bmatrix} = \sum_e \int_{\Omega_e} \begin{bmatrix} [G_u]^t \mathbb{e}^t [G_p] \\ [G_u]^t \mathbb{g}^t [G_a] \end{bmatrix} d\Omega \tag{12}$$

where $\mathbb{c}$, $\mathbb{p}$, $\mathbb{v}$, $\mathbb{e}$ and $\mathbb{g} = \mathbb{q}\mathbb{v}$ are material constants defined in (3), ρ_m is the mass density of the medium and Ω_e denotes the element e. The damping effect is introduced by Rayleigh's coefficients β and α in mechanical damping matrix $[\mathcal{C}]$.

By assuming that the reluctivity and elasticity are constant along the thickness of the thin magnetostrictive shell layer, it can be incorporated into the simulation using the following submatrices:

$$\begin{aligned} K_{aa}^{shell} &= \delta \nu_{11} \sum_e \int_{L_e} G_a^{shell^T} G_a^{shell} \, dl \\ K_{uu}^{shell} &= \delta c_{11} \sum_e \int_{L_e} G_u^{shell^T} G_u^{shell} \, dl_e \\ K_{ua}^{shell} &= \delta \sum_e \int_{L_e} G_u^{shell^T} \mathbb{g}^t G_a^{shell} dl_e \\ M^{shell} &= \delta \rho_v \sum_e \int_{L_e} N_{ui}^{0\,T} N_{ui}^0 \, dl_e \end{aligned} \tag{13}$$

where l_e denotes the line element domain.

The simulation uses the magnetic, electric, and elastic boundary conditions that were employed in the references [6], [7]. The external boundary of the domain is subject to Dirichlet conditions for the electric scalar potential, while the top and bottom limits are subjected to constant magnetic vector potentials to account for the applied external magnetic field. At the center of the composite, two fixed mechanical displacements are imposed, and the elastic problem is subject to the plane stress condition.

2.4. Nonlinear problem in static regime

A static ME problem is a complex problem that involves the nonlinear ferromagnetic properties of magnetostrictive materials, such as permeability and piezomagnetic coefficients, as well as the linear ferroelectric properties of piezoelectric materials, such as permittivity and piezoelectric coefficients. To simplify this problem, a proposed anhysteretic model for the Ni material is based on the magneto-elastic magnetization $M(H,T)$, which is defined as [12], and the magnetostriction strain $\lambda(H,T)$ is defined in [13]:

$$\begin{aligned} M(H,T) &= M_s \left(coth(z) - \frac{1}{z} \right) \\ \lambda(H,T) &= \lambda_s \left(1 - \frac{3 \cdot (coth(z) - \frac{1}{z})}{z} \right) \end{aligned} \tag{14}$$

with $z = \frac{\eta T}{H}$, and where M_s is the magnetization saturation, H is static magnetic field, T is an applied stress or a residual stress during fabrication process, η is a constant parameter that depends on the magnetic measurement data, and λ_s is the magnetostriction saturation.

Fig. 3 illustrates the strong agreement between the results obtained from the proposed model (14) and the magnetic hysteresis measurement of a freestanding nickel film isolated from the Ni/PZT-5H/Ni MEC.

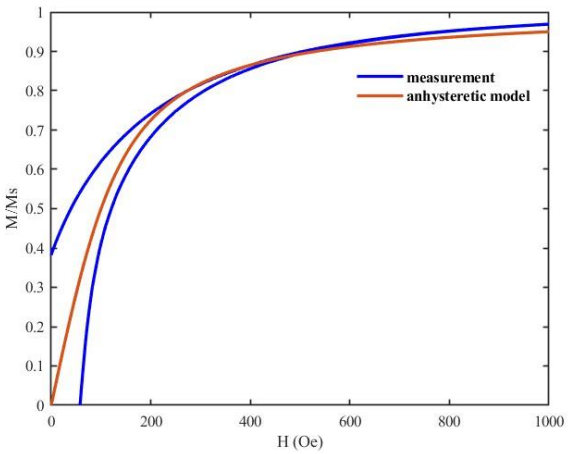

Fig. 3. Normalized magnetization curves of the Ni from measurement and the magneto-elastic model.

Additionally, Fig. 4 displays the piezomagnetic incremental coefficient $d_{33}{}^H = \partial_T M(H,T)$, and the relative permeability incremental coefficient $\mu_{33}{}^T = \mu_o + \partial_H M(H,T)$ predictions made by the model. Finally, by establishing the piezoelectric tensor $\boldsymbol{d^H}$ with $d_{33}{}^H$ and $d_{15}{}^H = 3\lambda(H,T)/H$ given in [14], and permeability tensor $\boldsymbol{\mu^T}$, respectively, the tensors $\mathbb{e}$ and $\mathbb{v}^S$ in equation (3) can be obtained using the relations $\mathbb{e} = \boldsymbol{d^H}\,\mathbb{c}^{\boldsymbol{B}}$ and $\mathbb{v}^S = (\boldsymbol{\mu^T} - \boldsymbol{d^H}\mathbb{c}^{\boldsymbol{B}}\boldsymbol{d^{H^T}})^{-1}$.

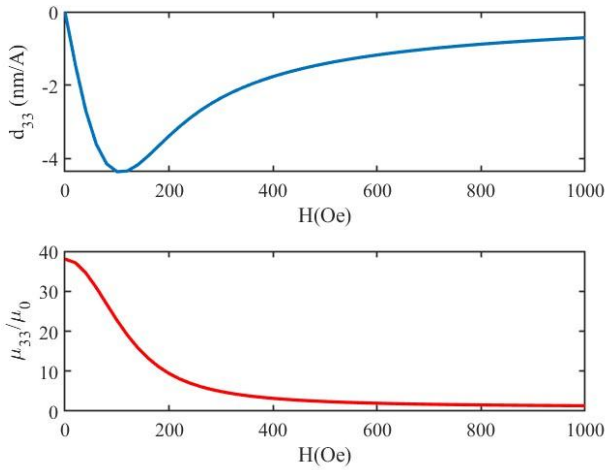

Fig. 4. Prediction of piezomagnetic $d_{33}{}^H$ and relative permeability $\mu_{33}{}^T/\mu_o$ incremental coefficients of the Ni.

2.5. Harmonic problem in dynamic regime

The matrix system in harmonic regime is given by (15) [6], [7]:

$$[\mathbb{K}]\{\mathcal{X}\} = \{\mathcal{F}\} \tag{15}$$

with $[\mathbb{K}] = \begin{bmatrix} K_{uu} - \omega^2 M + j\omega C_{uu} & K_{up} & 0 & K_{ua} \\ K_{pu} & K_{pp} & K_{pq} & 0 \\ 0 & K_{qp} & -j\omega Z & 0 \\ K_{au} & 0 & 0 & K_{aa} \end{bmatrix}$

and $\mathcal{X} = [\boldsymbol{u} \quad \boldsymbol{V} \quad Q \quad a_z]^T$, $\mathcal{F} = [0 \quad 0 \quad 0 \quad a_{ex}]^T$

where a_{ex} is the magnetic source of the excitation vector

The circuit equation relative to the influence of the electrical impedance load Z is considered in the global system $[\mathbb{K}]$ with the relation $\{\boldsymbol{V}\}K_{pq} - Zj\omega\{Q\} = 0$, where the electrical charge Q confined to the electrodes is an additional unknown and the incident vector K_{pq} is defined by:

$$K_{pq} = \begin{cases} \pm 1, \text{node} \in \text{electrodes} \\ 0, \text{else where} \end{cases} \quad (16)$$

3. SIMULATION AND MEASUREMENT

The simulations were conducted using a small applied signal δH_{ac} = 1 Oe, and a resistive load Z = 1 MΩ was connected between the Ni films, serving as the electrodes for each magnetoelectric composite (MEC). As depicted in Figure 5, our finite element method (FEM) analysis demonstrated good agreement between the magnetoelectric coefficients obtained from experimental measurements and simulations in both static and dynamic regimes for the Ni/PZT-5H/Ni MEC, employing the piezomagnetic and permeability models presented in Fig. 4. However, a discrepancy was observed between the simulated and experimental results for the Ni/(YXl)163˚ $LiNbO_3$/Ni MEC, which was attributed to the presence of magnetic anisotropy in the Ni films. To address this, we adjusted the parameter η in z in equation (14) based on magnetic hysteretic measurements and updated the piezomagnetic and permeability models accordingly. This adaptation led to an improved agreement between the simulation and experimental measurements, as demonstrated in Figure 6. The observed magnetic anisotropy issue was attributed to thermal residual stress generated during the RF sputtering process used for growing the Ni films [15]–[17]. This stress arises from the difference in the coefficient of thermal expansion (CTE) presented in Table 1 for the respective materials. Additionally, we observed that the remanent ME response α_E for the Ni/PZT-5H/Ni MEC was relatively weak at zero Hdc when compared to the Ni/(YXl)163˚ $LiNbO_3$/Ni composite, where it reached up to 80% of its maximum value. Thus, we concluded that the latter composite can be considered as a self-biased MEC.

Table 1. CTE of the materials in studied MECs.

Material	**CTE along length direction [K^{-1}]**	**CTE along width direction [K^{-1}]**
Ni	13×10^{-6}	13×10^{-6}
PZT-5H	4×10^{-6}	4×10^{-6}
(YXl)163˚ $LiNbO_3$	15.4×10^{-6}	8.18×10^{-6}

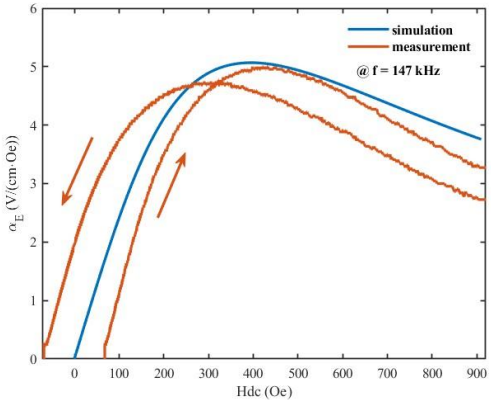

(a)

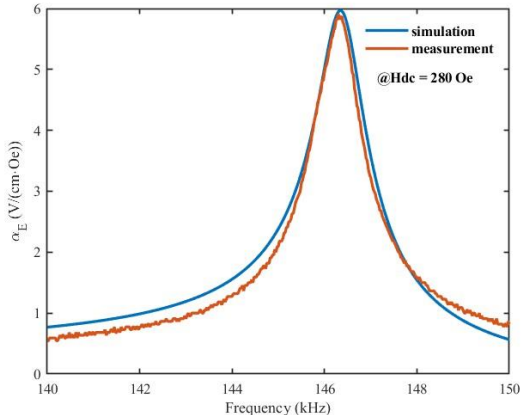

(b)

Fig. 5. ME coefficients results in static (a) and dynamic (b) regimes of Ni/PZT-5H/Ni.

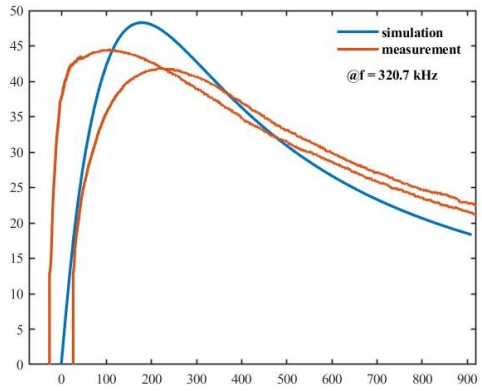

(a)

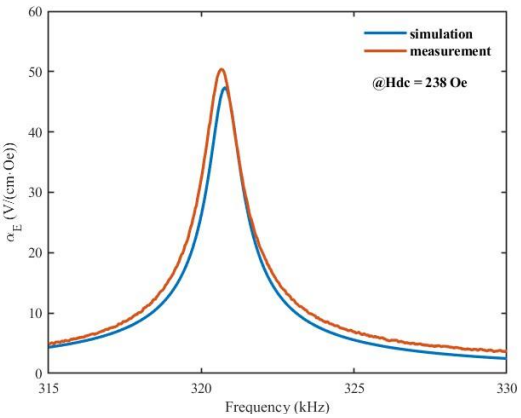

(b)

Fig. 6. ME coefficients results in static (a) and dynamic (b) regimes of Ni/(YXl)163˚ $LiNbO_3$/Ni.

4. CONCLUSIONS

This article proposes a FEM modeling approach using shell elements and a simplified magnetoelastic model to simulate thin magnetostrictive layers in magnetoelectric composites. This method offers computational time savings compared to traditional approaches and successfully simulates various composites, including Ni/PZT-5H/Ni and Ni/(YXl)163˚ $LiNbO_3$/Ni. The simulated results show good agreement with experimental measurements, although discrepancies arise in the Ni/(YXl)163˚ $LiNbO_3$/Ni composite due to magnetic anisotropy induced by residual stress in the Ni films. By adjusting the piezomagnetic and permeability parameters based on magnetic hysteretic measurements, the simulation achieves

improved agreement. The Ni/(YXl)163˚ $LiNbO_3$/Ni composite exhibits a self-biased characteristic with a significant remanent ME response. In summary, this work provides a valuable tool for investigating the performance of magnetoelectric composites featuring thin magnetostrictive layers, and can support the development of new ME devices with improved performance.

5. REFERENCES

[1] X. Liang, H. Chen, and N. X. Sun, 'Magnetoelectric materials and devices', *APL Materials*, vol. 9, no. 4, p. 041114, Apr. 2021, doi: 10.1063/5.0044532.

[2] C. M. Leung, J. Li, D. Viehland, and X. Zhuang, 'A review on applications of magnetoelectric composites: from heterostructural uncooled magnetic sensors, energy harvesters to highly efficient power converters', *J. Phys. D: Appl. Phys.*, vol. 51, no. 26, p. 263002, Jul. 2018, doi: 10.1088/1361-6463/aac60b.

[3] S. Kopyl, R. Surmenev, M. Surmeneva, Y. Fetisov, and A. Kholkin, 'Magnetoelectric effect: principles and applications in biology and medicine– a review', *Materials Today Bio*, vol. 12, p. 100149, Sep. 2021, doi: 10.1016/j.mtbio.2021.100149.

[4] K. Malleron, A. Gensbittel, H. Talleb, and Z. Ren, 'Experimental study of magnetoelectric transducers for power supply of small biomedical devices', *Microelectronics Journal*, vol. 88, pp. 184–189, Jun. 2019, doi: 10.1016/j.mejo.2018.01.013.

[5] Y. Zhou, D. Maurya, Y. Yan, G. Srinivasan, E. Quandt, and S. Priya, 'Self-Biased Magnetoelectric Composites: An Overview and Future Perspectives', *Energy Harvesting and Systems*, vol. 3, no. 1, pp. 1–42, Jan. 2016, doi: 10.1515/ehs-2015-0003.

[6] H. Talleb and Z. Ren, 'Finite element modeling of magnetoelectric laminate composites in considering nonlinear and load effects for energy harvesting', *Journal of Alloys and Compounds*, vol. 615, pp. 65–74, Dec. 2014, doi: 10.1016/j.jallcom.2014.06.121.

[7] H. Talleb and Z. Ren, 'Finite-Element Modeling of a Magnetoelectric Energy Transducer Including the Load Effect', *IEEE Trans. Magn.*, vol. 51, no. 3, pp. 1–5, Mar. 2015, doi: 10.1109/TMAG.2014.2357492.

[8] T. T. Nguyen, F. Bouillault, L. Daniel, and X. Mininger, 'Finite element modeling of magnetic field sensors based on nonlinear magnetoelectric effect', *Journal of Applied Physics*, vol. 109, no. 8, p. 084904, Apr. 2011, doi: 10.1063/1.3553855.

[9] R. C. Kambale, D.-Y. Jeong, and J. Ryu, 'Current Status of Magnetoelectric Composite Thin/Thick Films', *Advances in Condensed Matter Physics*, vol. 2012, pp. 1–15, 2012, doi: 10.1155/2012/824643.

[10] H. Talleb and Z. Ren, 'Mutliphysics Modeling of Thin Layer Magnetoelectric Laminate'.

[11] Zhuoxiang Ren, 'Degenerated Whitney prism elements-general nodal and edge shell elements for field computation in thin structures', *IEEE Trans. Magn.*, vol. 34, no. 5, pp. 2547–2550, Sep. 1998, doi: 10.1109/20.717587.

[12] V. Apicella, C. S. Clemente, D. Davino, and C. Visone, 'Experimental evaluation of external and built-in stress in Galfenol rods', *Physica B: Condensed Matter*, vol. 549, pp. 53–57, Nov. 2018, doi: 10.1016/j.physb.2017.09.081.

[13] H. Talleb and Z. Ren, 'A new nonlinear multiscale magnetostrictive approach for FEM modelling of magnetoelectric composites under magneto-thermo-elastic loading', *Composite Structures*, vol. 303, p. 116260, Jan. 2023, doi: 10.1016/j.compstruct.2022.116260.

[14] M. Hirao and H. Ogi, 'Coupling Mechanism', in *Electromagnetic Acoustic Transducers*, in Springer Series in Measurement Science and Technology. Tokyo: Springer Japan, 2017, pp. 15–38. doi: 10.1007/978-4-431-56036-4_2.

[15] M. Huff, 'Review Paper: Residual Stresses in Deposited Thin-Film Material Layers for Micro- and Nano-Systems Manufacturing', *Micromachines*, vol. 13, no. 12, p. 2084, Nov. 2022, doi: 10.3390/mi13122084.

[16] T. Truong *et al.*, 'Engineering Stress in Thin Films: An Innovative Pathway Toward 3D Micro and Nanosystems', *Small*, p. 2105748, Dec. 2021, doi: 10.1002/smll.202105748.

[17] S. A. Mathews and J. Prestigiacomo, 'Controlling magnetic anisotropy in nickel films on LiNbO3', *Journal of Magnetism and Magnetic Materials*, vol. 566, p. 170314, Jan. 2023, doi: 10.1016/j.jmmm.2022.170314.